Diamond & Related Materials 148 (2024) 111499

Contents lists available at ScienceDirect

Diamond & Related Materials

journal homepage: www.elsevier.com/locate/diamond

Development of hydrophobic graphenoid layer on Portland cement for non-thermal plasma method

N.G. Pereira Filho, E.P. Soares, J.C. Ferreira, R.F.B. de Souza *, D.A. Andrade, A.O. Neto

Instituto de Pesquisas Energéticas e Nucleares, IPEN/CNEN-SP, Av. Prof. Lineu Prestes, 2242 Cidade Universitária, CEP 05508-000 São Paulo, SP, Brazil

ARTICLE INFO

Keywords:
Hydrophobic covered
Graphenoid material
Portland cement
Non-thermal plasma
Impermeability enhancement
Nanomaterials
Surface modification

ABSTRACT

This study focuses on the development of hydrophobic layer on Portland cement using graphenoid materials to enhance impermeability and hydrophobicity. X-ray diffraction analysis indicated that characteristic peaks associated with concrete, such as ettringite, calcium hydroxide, and calcite, remained intact. The application of graphenoid material produced by non-thermal plasma resulted in the formation of carbonaceous structures, minimally affecting the overall cement structure. Raman spectroscopy provided detailed insights into the composition, highlighting the presence of specific and indicating boundary defects. Moreover, contact angle measurements confirmed a substantial increase in hydrophobicity for the graphene-coated cement, with an average angle of 117° ± 4.72° demonstrated graphenoid material layers deposited over structural defects, effectively waterproofing and enhancing local hydrophobicity.

1. Introduction

Concrete is universally acclaimed as one of the most versatile, durable, and robust construction materials in the world. While permeability is desirable for concrete in paving applications, facilitating water drainage [1], water infiltration into concrete used for structural purposes can lead to structural decay and aesthetic concerns, ultimately diminishing the longevity of concrete structures [2,3]. This infiltration not only jeopardizes the structural integrity of concrete but also gives rise to issues such as reinforcement corrosion and premature degradation.

In response to these challenges, there has been a burgeoning interest in developing additives that enhance the waterproofing characteristics of concrete, with the goal of extending the service life of concrete elements while simultaneously reducing the costs associated with repairs and maintenance [3,4]. Among various techniques, surface coatings have emerged as the predominant method adopted by a majority of researchers, often evaluated through water absorption tests. This research trend highlights a notable emphasis on the utilization of polymer-based materials, silicate-containing compounds, silanes, siloxanes, cementitious materials, and specific nanomaterials. As a result, additives can be classified into three categories based on their material composition, application methodology, and functional attributes [5,6]. The addition of these materials to concrete introduces issues of brittleness and rehydration during consolidation. An alternative approach is the application in the form of a coating on the already cured concrete [7,8]. However, this method requires an adhesive component based on resins and solvents, resulting in higher material consumption.

Graphene, renowned for its water-repellent properties and its ability to enhance impermeability [9–11], represents a promising solution to the evolving demands of modern civil construction. It offers the potential for developing cost-effective graphene material layers capable of efficiently repelling water. Nevertheless, it is important to note that graphene remains a relatively expensive material, often applied as an additive to polymer coatings [12,13]. However, the development of low-cost graphene production technologies has significantly bolstered the attractiveness and feasibility of incorporating graphene in construction applications.

In plasma-based methodologies [14,15], small graphene flakes comprising only a few layers can be synthesized without the need for substrates, utilizing a rapid and precisely controlled synthesis process. Plasma synthesis entails the decomposition of a carbon source, leading to the formation of carbon particle fragments within the gaseous phase of the plasma stream.

Recently, Neto et al.'s research group [16–18] introduced a clean, rapid, and cost-effective methodology for growing graphene nanoparticles on non-conductive materials such as hexagonal boron nitride and fiberglass. This approach involves the conversion of hydrocarbons

* Corresponding author.
E-mail address: souza.rfb@gmail.com (R.F.B. de Souza).

https://doi.org/10.1016/j.diamond.2024.111499
Received 4 March 2024; Received in revised form 12 June 2024; Accepted 12 August 2024
Available online 14 August 2024

into graphene-like materials using a cold plasma generator. Significantly, this method enables the direct growth of graphene onto substrates without the need for additional adhesion-promoting substances. In light of these advancements, this study primarily aims to investigate the application of a bottom-up graphene formation method on Portland cement substrates to enhance their waterproofing capabilities. The research seeks to demonstrate the effectiveness of this approach in creating a hydrophobic layer that increases the cement's resistance to water infiltration, thereby extending the durability of concrete structures.

2. Experimental

The Portland cement used in this study was Type I. A paste was prepared with a water-to-cement (w/c) ratio of 0.5. The mixture was thoroughly homogenized and then poured into sample holders measuring approximately 20 mm × 20 mm × 5 mm. After setting, the samples were demoulded after 24 h and cured at room temperature.

The deposition of graphene onto the Portland cement samples was achieved using a non-thermal plasma generator coupled to a reaction vessel, as detailed in previous studies [16–18]. Cyclohexane (Aldrich) was used as the carbon source. The plasma process involved initiating a 60 kV electric arc with a flow of nitrogen gas (N2) at room temperature between a 316 L steel electrode and another electrode made of 316 L steel wire, on which the Portland cement sample was affixed. The process continued until the complete evaporation and conversion of the cyclohexane.

The resulting dry material was characterized using scanning electron microscopy (SEM). A Jeol JSM-6701F instrument was employed for this purpose. The samples were transversely cut using an Isomet 900 cutter equipped with a diamond blade for ceramic materials, operating at a cutting speed of 100 rpm without cooling to preserve the integrity of the graphene deposit.

X-ray diffraction (XRD) patterns were obtained using a Miniflex II diffractometer equipped with a Cu Kα radiation source (wavelength of 0.15406 Å). The scans were performed over a 2θ range of 2–90° at a scan speed of 2° per minute.

Raman spectra were recorded using a Horiba Scientific MacroRam Raman spectroscopy apparatus with a 785 nm laser. This technique provided insights into the molecular composition and structural changes in the cement matrix due to the graphene coating.

Contact angle measurements were conducted following the ISO 15989/2004 methodology using a goniometer (KINO-SL150E). For each substrate, 2.0 μL deionized water droplets were placed on the sample surfaces. Multiple measurements were taken on at least five distinct samples, with ten readings per sample, and the average contact angles were recorded.

3. Results and discussion

In Fig. 1a and b, cross-sectional views of hardened Portland cement and the same cement, which was covered with graphenoid material obtained through non-thermal plasma treatment, are presented. For the sample treated with carbonaceous material, a darker region is evident, indicating penetration of up to approximately 70 μm. When was switch to secondary electron imaging to examine the same region, we observe structural alterations on the material's surface, extending to around 120 to 150 μm. This altered region exhibits a softer texture compared to the bulk material, as depicted in Fig. 1c. The soft texture becomes more evident upon closer examination, as seen in Fig. 1d, e, and f. These structural modifications can be attributed to the non-thermal plasma process, which has previously demonstrated its effectiveness in altering stable structures such as SiO_2 and h-BN [17,18].

Fig. 2 shows XRD patterns of the PC with and without graphenoid layer, and is possible to observe all characteristic peaks of the Portland cement, these peaks are related to the presence of ettringite at around 2θ ~ 23°, 31°, and 33°, resulting from the sulphate ion's reaction with calcium-bearing compounds. Calcite, with its characteristic peak at ~26°, is the primary hydration product in cement composites and is also present in gypsum compounds [19]. Other notable peaks include portlandite at 48° [20], quartz around ~38° and 52° [21], alite at ~29°, 32°, and 62° degrees, convoluted at ~30° and 33° from belite, and calcium hydroxide at ~18°, 34°, and 47° degrees [22]. In the absence of peak shifts, these results suggest that the structure was largely unaffected by the non-thermal plasma treatment, except for the absence of the 18° peak in the coated sample.

Additionally, the method of depositing graphenoid nanoflakes via non-thermal plasma on cement results in the formation of carbonaceous structures with a few layers [16,17], which can render carbon phases not directly observable through X-ray diffraction for certain materials, primarily due to differences in crystallite size. As depicted in Fig. 2b, the XRD pattern was plotted on a logarithmic scale to investigate the potential presence of graphene within the concrete sample. Examination of the graphene's crystallographic pattern reveals indications of nanoflakes stacking and crystalline dimensions within the graphene crystal lattice. These distinctive characteristics manifest in the (002) and (100) planes, which display diffraction peaks approximately at 2θ ~ 21.3° and 24.9° [16], respectively, in conjunction with the diffraction peaks corresponding to the cement phases.

Utilizing Raman spectroscopy (Fig. 3), an array of distinct spectral bands within Portland Cement was discerned. Specifically, prominent bands corresponding to ettringite at 1160 cm^{-1} [23], and a noteworthy band at 1440 cm^{-1}, associated with ettringite $Ca_6Al_2O_6(SO_4).14H_2O$ and linked to the sulphate $\nu_2SO_4^{2-}$ mode [24]. Furthermore, the spectral analysis revealed discernible bands at 1485 cm^{-1} and 1765 cm^{-1}, denoting the presence of calcium hydroxide [25], and a band at 1249 cm^{-1}, correlated with $Ca.H_2O_5Si^{2-}$ [26]. Noteworthy contributions also included a distinctive signature at 1624 cm^{-1} for calcium oxide [27], a discernible peak at 1680 cm^{-1} attributable to $3CaO.Al_2O_3$ [28], and a band at 1085 cm^{-1} [29]. The latter was ascribed to calcite (1070 cm^{-1}) [30], while alternatively, the peak at 1081 cm^{-1} was associated with the symmetrical stretching mode of Si—O tetrahedra [31], it is imperative to underscore that these proposed identifications are not mutually exclusive; rather, the observed spectrum may encompass a combination thereof.

Upon scrutinizing the Covered Portland Cement sample, a conspicuous suppression of the majority of bands associated with Portland Cement became evident. Instead, distinctive peaks corresponding to the D1, D2, D3, and G modes of carbon at approximately 1322, 1623, 1495, and 1587 cm^{-1}, respectively, were observed [32]. These outcomes provide clear evidence of a partial coverage overlaying the Portland Cement substrate.

The literature extensively discusses the G-band, which corresponds to the first-order scattering of the E_{2g} mode associated with sp^2 carbon. Additionally, the D band can be attributed to structural defects, carbon amorphism, or edge defects, all of which have the potential to disrupt symmetry and selection rules [33]. The G band's characteristics are influenced by the number of layers, reflecting the contribution of the vibrational mode involving more carbon atoms. Changes in its intensity, shape, and position serve as indicators of induced deformations. Notably, within the literature, the Raman intensity ratio of the D-band to G-band (I_D/I_G) stands as a pivotal parameter for assessing the degree of disorder in graphene [34]. In the case of this sample, the obtained value of 3.5 signifies the presence of boundary defects.

The hydrophobicity was assessed through contact angle measurements (Fig. 4), yielding an average angle of 117° ± 4.72°, in stark contrast to the behavior observed in plain Portland cement, where water droplets are readily absorbed, while the nanocarbon-coated material remains impermeable [35,36]. This result is in agreement with the observed in Fig. 1, where we observe layers of graphenoid materials deposited on the defects of the cement structure, rendering it impermeable and increasing local hydrophobicity. The application of

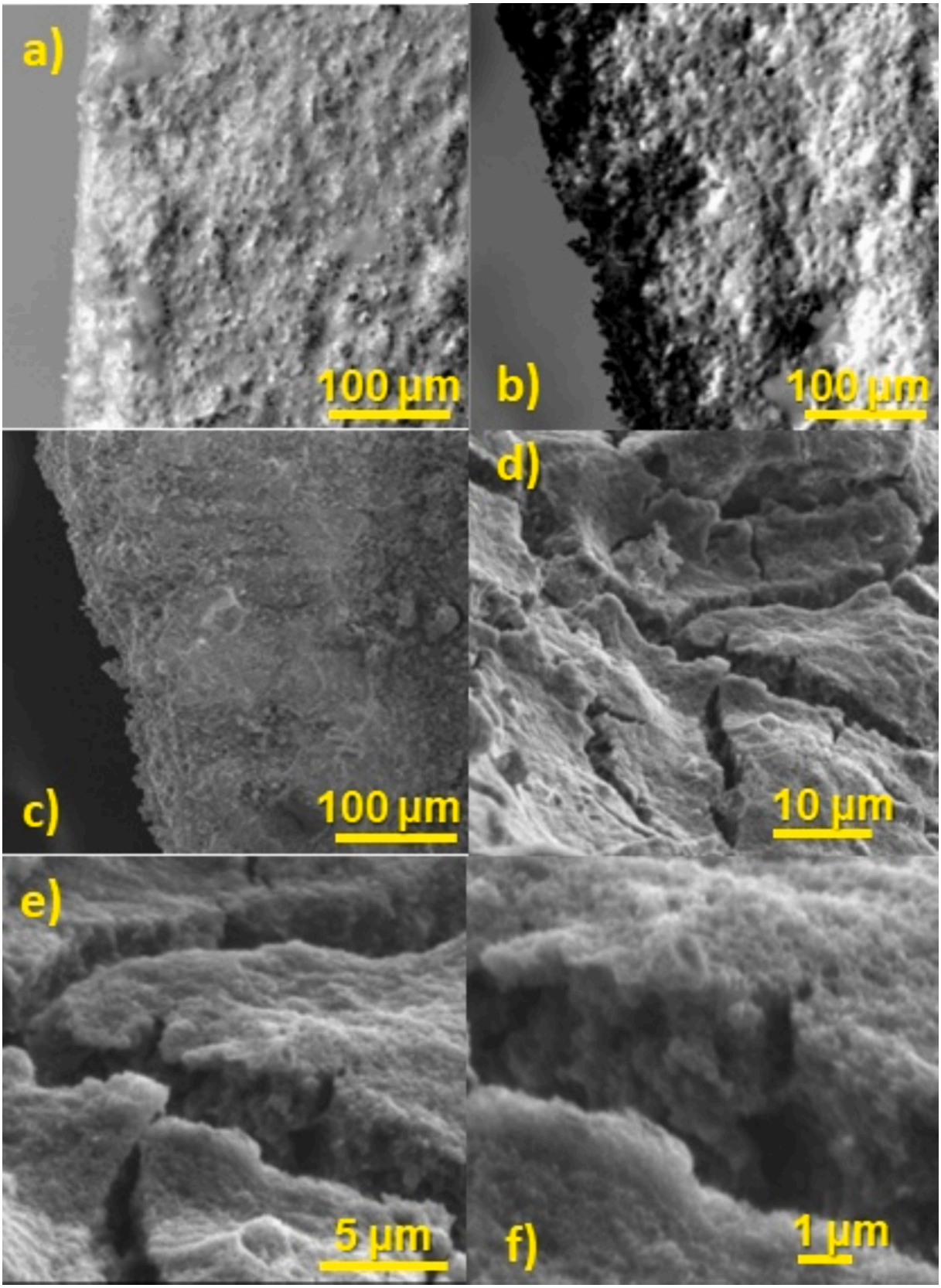

Fig. 1. SEM images of a) Portland Cement, b) Covered Portland Cement, c) SEI of Covered Portland Cement with a magnification of 250×, d) 2000×, e) 5000×, and f) 10,000×.

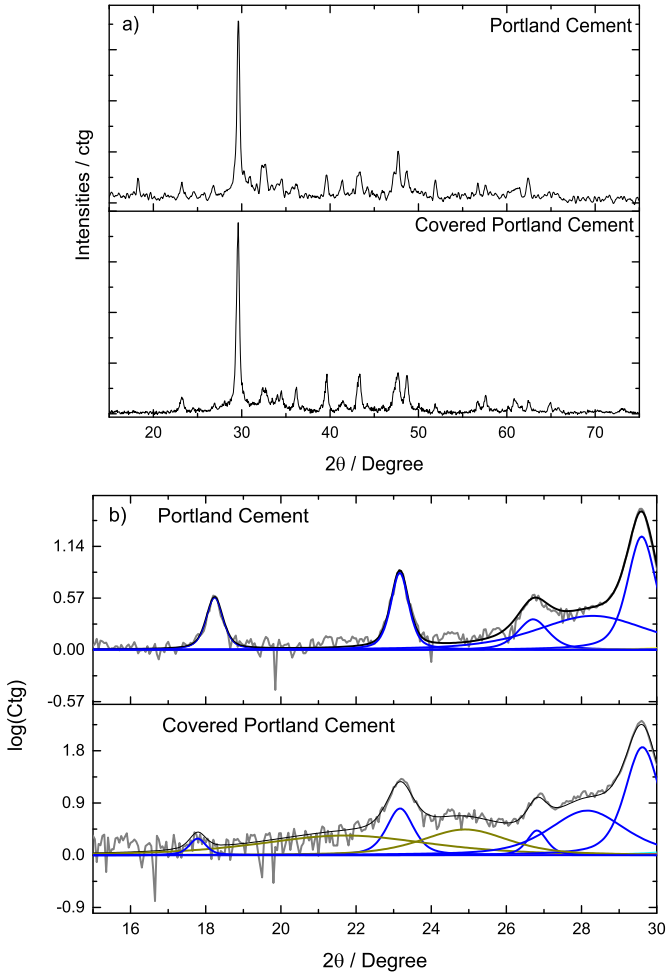

Fig. 2. a) X-ray diffraction patterns of Portland Cement and Covered Portland Cement. b) Logarithm of the intensities obtained from the X-ray diffraction patterns measured for Portland Cement, with deconvolution of the peak corresponding to the (002) plane, as well as carbon diffraction.

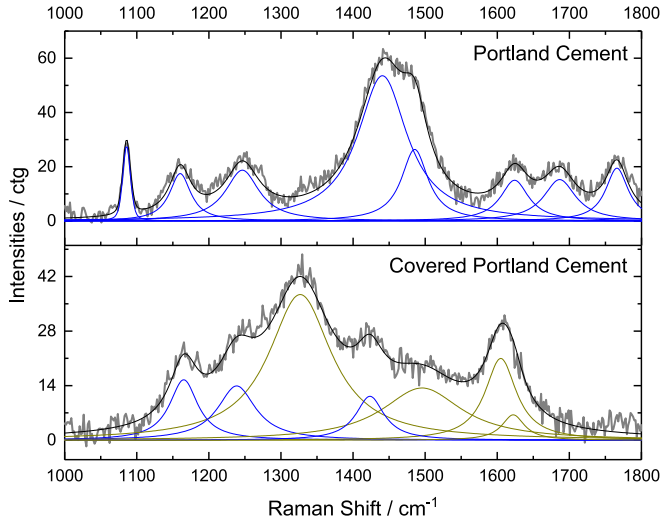

Fig. 3. Raman Spectrum of the Portland Cement and Covered Porland Cement deconvolved in range of 1000 and 1800 cm^{-1}. In blue the cement bands and in dark yellow the carbon bands.

graphene to the Portland cement surface has brought about a remarkable shift in wettability characteristics. This substantial increase in the contact angle, indicative of enhanced hydrophobicity due to graphene application [9], underscores the beneficial impact of the coating on the cement surface. Such a modification in wettability properties carries significant implications for bolstering water infiltration resistance and augmenting the durability of concrete structures.

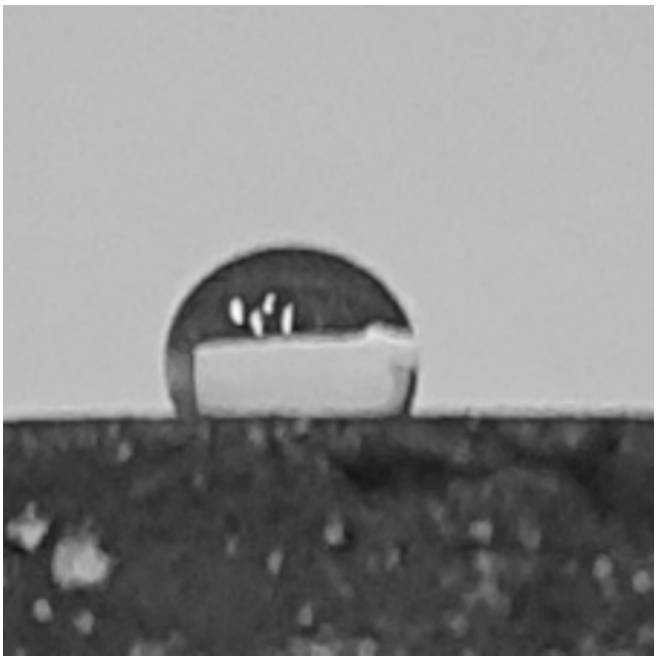

Fig. 4. Contact angle result image of Covered Portland Cement.

4. Conclusion

The application of a bottom-up graphene formation method using non-thermal plasma on Portland cement substrates, aimed at enhancing their waterproofing capabilities. The X-ray diffraction analysis revealed that the characteristic peaks of the cement remained evident, indicating the presence of ettringite and other typical Portland cement phases, with no significant structural changes due to the non-thermal plasma treatment. The formation of the graphene-like film via non-thermal plasma resulted in the creation of carbonaceous structures with a few layers on the Portland cement. Raman spectroscopy provided valuable insights into the concrete's composition, identifying distinct spectral bands of ettringite, calcium hydroxide, calcite, and other phases. The Raman intensity ratio of the D-band to G-band (ID/IG) value of 3.5 indicated the presence of boundary defects, suggesting the formation of graphene with some imperfections. Contact angle measurements confirmed a significant increase in hydrophobicity and impermeability in contrast to the immediate absorption of water droplets by untreated Portland cement. This substantial increase in the contact angle, indicative of enhanced hydrophobicity due to graphene application, underscores the beneficial impact of the coating on the cement surface. These findings are promising for enhancing the durability and longevity of concrete structures, especially in scenarios where water infiltration poses a significant challenge.

CRediT authorship contribution statement

N.G. Pereira Filho: Methodology, Investigation, Data curation. **E.P. Soares:** Methodology, Investigation, Data curation, Conceptualization. **J.C. Ferreira:** Methodology, Investigation, Data curation. **R.F.B. de Souza:** Writing – original draft, Validation, Methodology. **D.A. Andrade:** Writing – original draft, Supervision, Project administration,

Conceptualization. **A.O. Neto:** Writing – original draft, Supervision, Project administration, Methodology, Funding acquisition, Conceptualization.

Declaration of competing interest

The authors declare that they have no known competing financial interests or personal relationships that could have appeared to influence the work reported in this paper.

Data availability

Data will be made available on request.

Acknowledgment

We are grateful to CAPES, CNPq (350514/2023-2, 302709/2020-7), COPDE/IPEN (2020.06.IPEN.05), for financial supports.

References

[1] N. Xie, M. Akin, X. Shi, Permeable concrete pavements: a review of environmental benefits and durability, J. Clean. Prod. 210 (2019) 1605–1621, https://doi.org/10.1016/j.jclepro.2018.11.134.
[2] X. Xiao, J. Li, D. Cai, H. Cheng, F. Xiao, Characterizing thermal fatigue behaviors of asphalt concrete waterproofing layer in high-speed railway using customized overlay test, Int. J. Fatigue 165 (2022) 107176, https://doi.org/10.1016/j.ijfatigue.2022.107176.
[3] N.Z. Muhammad, A. Keyvanfar, M.Z.Abd. Majid, A. Shafaghat, J. Mirza, Waterproof performance of concrete: a critical review on implemented approaches, Construct. Build Mater. 101 (2015) 80–90, https://doi.org/10.1016/j.conbuildmat.2015.10.048.
[4] A. Garbacz, M. Górka, L. Courard, Effect of concrete surface treatment on adhesion in repair systems, Mag. Concr. Res. 57 (2005) 49–60, https://doi.org/10.1680/macr.2005.57.1.49.
[5] P.A.M. Basheer, L. Basheer, D.J. Cleland, A.E. Long, Surface treatments for concrete: assessmentmethods and reported performance, Construct. Build Mater. 11 (1997) 413–429, https://doi.org/10.1016/S0950-0618(97)00019-6.
[6] M. Horgnies, P. Willieme, O. Gabet, Influence of the surface properties of concrete on the adhesion of coating: characterization of the interface by peel test and FT-IR spectroscopy, Prog. Org. Coat. 72 (2011) 360–379, https://doi.org/10.1016/j.porgcoat.2011.05.009.
[7] F. Wang, T. Xie, S. Lei, J. Ou, W. Li, M. Xue, D. Huang, Preparation and properties of foundry dust/Portland cement based composites and superhydrophobic coatings, Construct. Build Mater. 246 (2020) 118466, https://doi.org/10.1016/j.conbuildmat.2020.118466.
[8] S. Yao, C. Hu, F. Wang, S. Hu, Improving the interfacial properties of PVA fiber and cementitious composite: design and characterization, Construct. Build Mater. 409 (2023) 134163, https://doi.org/10.1016/j.conbuildmat.2023.134163.
[9] O. Leenaerts, B. Partoens, F.M. Peeters, Water on graphene: hydrophobicity and dipole moment using density functional theory, Phys. Rev. B 79 (2009) 235440, https://doi.org/10.1103/PhysRevB.79.235440.
[10] Z. Zhou, S. Li, J. Cao, X. Chen, Z. Wu, P. Zhou, The waterproofing effect and mechanism of graphene oxide/silane composite emulsion on cement-based materials under compressive stress, Construct. Build Mater. 308 (2021) 124945, https://doi.org/10.1016/j.conbuildmat.2021.124945.
[11] Q.G. Jiang, Z.M. Ao, D.W. Chu, Q. Jiang, Reversible transition of graphene from hydrophobic to hydrophilic in the presence of an electric field, J. Phys. Chem. C 116 (2012) 19321–19326, https://doi.org/10.1021/jp3050466.
[12] Y. Zhang, S. Li, W. Zhang, X. Chen, D. Hou, T. Zhao, X. Li, Preparation and mechanism of graphene oxide/isobutyltriethoxysilane composite emulsion and its effects on waterproof performance of concrete, Construct. Build Mater. 208 (2019) 343–349, https://doi.org/10.1016/j.conbuildmat.2019.03.015.
[13] X. Chen, Y. Zhang, S. Li, Y. Geng, D. Hou, Influence of a new type of graphene oxide/silane composite emulsion on the permeability resistance of damaged concrete, Coatings (2021), https://doi.org/10.3390/coatings11020208.
[14] A. Dato, Graphene synthesized in atmospheric plasmas—a review, J. Mater. Res. 34 (2019) 214–230, https://doi.org/10.1557/jmr.2018.470.
[15] M.B. Shavelkina, E.A. Filimonova, R.K. Amirov, Effect of helium/propane–butane atmosphere on the synthesis of graphene in plasma jet system, Plasma Sources Sci. Technol. 29 (2020) 025024, https://doi.org/10.1088/1361-6595/ab61e3.
[16] P.V.R. Gomes, N.F.B. Azeredo, L.M.S. Garcia, P.J. Zambiazi, G.R. Morselli, R. A. Ando, L. Otubo, D.R.R. Lazar, R.F.B. de Souza, D.F. Rodrigues, A.O. Neto, Layered graphene/hexagonal boron nitride nanosheets (Gr/h-BNNs) applied to the CO2 photoconversion into methanol, Appl. Mater. Today 29 (2022) 101605, https://doi.org/10.1016/j.apmt.2022.101605.
[17] P.V.R. Gomes, R.N. Bonifacio, B.P.G. Silva, J.C. Ferreira, R.F.B. de Souza, L. Otubo, D.R.R. Lazar, A.O. Neto, Graphene deposited on glass fiber using a non-thermal plasma system, Eng (2023) 2100–2109, https://doi.org/10.3390/eng4030119.
[18] R.F.B. de Souza, V.A. Maia, P.J. Zambiazzi, L. Otubo, D.R.R. Lazar, A.O. Neto, Facile, clean and rapid exfoliation of boron-nitride using a non-thermal plasma process, Mater. Today Adv. 12 (2021) 100181, https://doi.org/10.1016/j.mtadv.2021.100181.
[19] K. Chintalapudi, R.M.R. Pannem, Enhanced chemical resistance to sulphuric acid attack by reinforcing graphene oxide in ordinary and Portland Pozzolana cement mortars, Case Stud. Constr. Mater. 17 (2022) e01452, https://doi.org/10.1016/j.cscm.2022.e01452.
[20] V.D. Ho, C.-T. Ng, T. Ozbakkaloglu, A. Goodwin, C. McGuckin, R.U. Karunagaran, D. Losic, Influence of pristine graphene particle sizes on physicochemical, microstructural and mechanical properties of Portland cement mortars, Construct. Build Mater. 264 (2020) 120188, https://doi.org/10.1016/j.conbuildmat.2020.120188.
[21] S. Du, Z. Tang, J. Zhong, Y. Ge, X. Shi, Effect of admixing graphene oxide on abrasion resistance of ordinary Portland cement concrete, AIP Adv. 9 (2019), https://doi.org/10.1063/1.5124388.
[22] V.D. Ho, C.-T. Ng, C.J. Coghlan, A. Goodwin, C. Mc Guckin, T. Ozbakkaloglu, D. Losic, Electrochemically produced graphene with ultra large particles enhances mechanical properties of Portland cement mortar, Construct. Build Mater. 234 (2020) 117403, https://doi.org/10.1016/j.conbuildmat.2019.117403.
[23] J. Bensted, Uses of Raman spectroscopy in cement chemistry, J. Am. Ceram. Soc. 59 (1976) 140–143, https://doi.org/10.1111/j.1151-2916.1976.tb09451.x.
[24] R. Masmoudi, K. Kupwade-Patil, A. Bumajdad, O. Büyüköztürk, In situ Raman studies on cement paste prepared with natural pozzolanic volcanic ash and ordinary Portland cement, Construct. Build Mater. 148 (2017) 444–454, https://doi.org/10.1016/j.conbuildmat.2017.05.016.
[25] F. Liu, Z. Sun, C. Qi, Raman spectroscopy study on the hydration behaviors of Portland cement pastes during setting, J. Mater. Civ. Eng. 27 (2015) 04014223, https://doi.org/10.1061/(ASCE)MT.1943-5533.0001189.
[26] M. Azeem, M.A. Saleem, A Raman spectroscopic study of calcium silicate hydrate (CSH) in the cement matrix with CNTs and oxide additives, J. Spectrosc. 2022 (2022) 2281477, https://doi.org/10.1155/2022/2281477.
[27] G. Ovcharenko, E. Ibe, A.J.E.S.W.C. Viktorov, Assessment of the Influence of Additives in Concrete by the Raman Spectroscopy Method 157, 2020 (06004).
[28] J.J. Soto-Bernal, R. Gonzalez-Mota, I. Rosales-Candelas, J.A. Ortiz-Lozano, Effects of static magnetic fields on the physical, mechanical, and microstructural properties of cement pastes, Adv. Mater. Sci. Eng. 2015 (2015) 934195, https://doi.org/10.1155/2015/934195.
[29] I.G. Richardson, J. Skibsted, L. Black, R.J. Kirkpatrick, Characterisation of Cement Hydrate Phases by TEM, NMR and Raman Spectroscopy 22, 2010, pp. 233–248, https://doi.org/10.1680/adcr.2010.22.4.233.
[30] N. Garg, K. Wang, S.W. Martin, A Raman spectroscopic study of the evolution of sulfates and hydroxides in cement–fly ash pastes, Cem. Concr. Res. 53 (2013) 91–103, https://doi.org/10.1016/j.cemconres.2013.06.009.
[31] M. Vetter, J. Gonzalez-Rodriguez, E. Nauha, T. Kerr, The use of Raman spectroscopy to monitor phase changes in concrete following high temperature exposure, Construct. Build Mater. 204 (2019) 450–457, https://doi.org/10.1016/j.conbuildmat.2019.01.165.
[32] Z. Lu, C. Wang, X. Chen, M. Song, W. Xia, Effects of buffer gas on N-doped graphene in a non-thermal plasma process, Diamond Relat. Mater. 118 (2021) 108548, https://doi.org/10.1016/j.diamond.2021.108548.
[33] J.-B. Wu, M.-L. Lin, X. Cong, H.-N. Liu, P.-H. Tan, Raman spectroscopy of graphene-based materials and its applications in related devices, Chem. Soc. Rev. 47 (2018) 1822–1873, https://doi.org/10.1039/C6CS00915H.
[34] A.C. Ferrari, D.M. Basko, Raman spectroscopy as a versatile tool for studying the properties of graphene, Nat. Nanotechnol. 8 (2013) 235–246, https://doi.org/10.1038/nnano.2013.46.
[35] J.S. Bunch, S.S. Verbridge, J.S. Alden, A.M. van der Zande, J.M. Parpia, H. G. Craighead, P.L. McEuen, Impermeable atomic membranes from graphene sheets, Nano Lett. 8 (2008) 2458–2462, https://doi.org/10.1021/nl801457b.
[36] S. Rahpeima, E.M. Dief, S. Ciampi, C.L. Raston, N. Darwish, Impermeable graphene oxide protects silicon from oxidation, ACS Appl. Mater. Interfaces 13 (2021) 38799–38807, https://doi.org/10.1021/acsami.1c06495.